Robust Belief Roadmap: Planning Under Uncertain And Intermittent Sensing

Shaunak D. Bopardikar Brendan J. Englot Alberto Speranzon

Abstract— **This paper considers the problem of planning a path for an autonomous vehicle from a start to a goal location in presence of sensor intermittency modeled as a stochastic process, in addition to process and measurement noise. The aim is to plan a path that minimizes the localizational uncertainty for the vehicle upon arriving at the goal location. The main contribution of this paper is two-fold. We first show that it is possible to obtain an analytical bound on the performance of a state estimator under sensor misdetection (intermittency) occurring stochastically over time. We then use this bound in a sample-based path planning algorithm to produce a path that trades off accuracy and robustness. This extends the recent body of work on planning under uncertainty to include the fact that sensors may not provide any measurement owing to misdetection. This is caused either by adverse environmental conditions that prevent the sensors from making measurements or by the fundamental limitations of the sensors. Examples include RF-based ranging devices that intermittently do not receive the signal from beacons because of obstacles or the misdetection of features by a camera system in detrimental lighting conditions. Computational results demonstrate the benefit of the approach and comparisons are made with the state of the art in path planning in belief space.**

Index Terms— **Path planning, Belief space planning, Autonomous systems, Localization.**

I. Introduction

Map-based, GPS-denied navigation often relies on the measurement of environmental features to perform state estimation. Whether these features are extracted from camera or LIDAR data, or supplied by range beacons, their measurement will be corrupted by noise and, in general, intermittent. Examples of such situations include RF-based ranging devices that intermittently do not receive signals from beacons because of obstacles and misdetection of features by a camera system in textureless areas of the environment and/or due to adverse lighting conditions. Although sensor fusion can mitigate the intermittency, it is clear that one would like the vehicle to navigate in regions of the environment where the intermittency is lower and/or where it is more likely that a large number of sensors are producing measurements. As prior maps are becoming increasingly rich and sensor-environment interactions can be simulated with reasonable fidelity, one can argue that a model for the intermittency process may be available. Also, subsets of data collected in various environmental situations can provide data to infer model parameters.

In this context, the main contribution of this paper is twofold. We first show that it is possible to obtain an analytical bound on the performance of a state estimator under sensor misdetection occurring stochastically over time. We then use this bound in a sample-based path planning algorithm to produce a path that trades off accuracy and robustness.

Recent work in robotics has emphasized robust path planning under various sources of uncertainty. The stochastic motion roadmap is a foundational work in modeling path planning under process noise as a Markov decision process (MDP), which is solved optimally using dynamic programming [1]. Using the framework of Partially Observable Markov Decision Processes (POMDP), Marthi, in [2] addresses path planning in environments in which obstacles appear/disappear dynamically over time.

If stochastic measurements are considered in addition to actions, the planning problem, also a POMDP, is intractable for relevant problems in robotics. As a result, a variety of algorithms make simplifying assumptions and find high-quality feasible paths that manage uncertainty. Sample-based motion planning is often utilized to generate a set of collision-free feasible paths from which a minimum-uncertainty path is selected. The belief roadmap (BRM) [3] builds a probabilistic roadmap (PRM) [4] in a robot's state space, propagates beliefs over the roadmap using an extended Kalman filter (EKF) [5], and plans a path of minimum goal-state uncertainty. This approach has been extended in [6] to bias the PRM samples using a Sensory Uncertainty Field (SUF) [7], which expresses the spatial variation in sensor performance over the workspace. Rapidly-exploring random belief trees (RRBTs) [8] use the EKF to propagate belief states over a rapidly-exploring random graph (RRG) [9], to find asymptotically optimal paths that minimize goal-state uncertainty subject to chance constraints. Linear quadratic Gaussian motion planning (LQG-MP) [10] pairs an LQG controller-estimator duo with trajectories planned using rapidly-exploring random trees (RRTs) [11], seeking a path that minimizes the product of collision probabilities at all states. Instead of sample-based planning, continuous optimization is used by Platt *et al.* [12]; locally optimal paths are computed directly in belief space under the assumption that the maximum-likelihood measurement is always obtained, and LQG estimation and control are applied.

Map uncertainty is combined with assumptions of uncertain actions and measurements by Kurniawati *et al.* [13], who use a point-based POMDP planner to obtain an approximate minimum-cost solution, where the cost is a combination of movement and collision risk. A hierarchical approach is adopted by Vitus *et al.* [14], who manage uncertainty by decomposing the workspace into a graph and optimizing over

The authors are with United Technologies Research Center. This work was supported by United Technologies Research Center under the Autonomy initiative. Email: {BopardSD, EnglotBJ, SperanA}@utrc.utc.com.

the graph in several steps. Wellman *et al.* [15] consider a setting in which the edge costs on the graph are uncertain and provide a path planning algorithm that produces optimal paths under time-dependent uncertainty. Acar *et al.* [16] present an approach that uses geometric and topological features instead of sensor uncertainty models.

In total, we consider three sources of uncertainty: process noise, sensor noise, and sensor intermittency, for which sensor misdetections occur with a known probability. We demonstrate that choosing the expected maximum eigenvalue of the error covariance matrix as a metric we can obtain a novel upper bound on its evolution in the case of stochastic misdetections by the robot's sensors. In the case of no misdetection, these bounds are distinct from existing results in the literature, surveyed in [17], which are mainly for the Algebraic Riccati equation, representing the steady state value of the expected error covariance instead of its instantaneous value that we are concerned with. Other metrics, such as the trace of the expected error covariance matrix, have been commonly considered in the past, cf. [3]. However, to the best of our knowledge, the trace does not offer a tractable means to bound its evolution over time in the stochastic setting of sensor misdetections. Although the maximum eigenvalue introduces conservativeness, the proposed analytical bound (scalar) offers computational advantages, especially when the search space is large.

This paper is organized as follows. In Section II, we formulate the problem. An analytical bound on the performance of the state estimator with probabilistic sensor misdetections is derived in Section III. In Section IV, we describe in detail how the analytical bound is used for robust path planning. Computational results are reported in Section V. Finally, conclusions and future directions are discussed in Section VI.

II. Problem Formulation

We consider a general model of an agent whose state evolves as per a non-linear discrete-time dynamical system

$$\mathbf{x}(t+1) = \mathbf{f}(\mathbf{x}(t), \mathbf{n}(t)), \tag{1}$$

where $\mathbf{x} \in \mathbb{R}^{n_x}$ is the state describing the system at time t, $\mathbf{f} : \mathbb{R}^{n_x} \times \mathbb{R}^{n_n} \to \mathbb{R}^{n_x}$ describes the state transition map of the system and $\mathbf{n} \in \mathbb{R}^{n_n}$ is the process noise. The agent is equipped with m sensors (alternatively, can distinguish between information received from m different sources) in order to estimate the state $\mathbf{x}$. Sensor output is modeled as

$$\mathbf{y}_j(t) = \mathbf{h}_j(\mathbf{x}(t), \mathbf{v}_j(t)), \qquad \forall j \in \{1, \dots, m\}, \tag{2}$$

where $\mathbf{v}_j \in \mathbb{R}^{n_j}$ is the measurement noise of the j-th sensor and $\mathbf{h} : \mathbb{R}^{n_x} \times \mathbb{R}^{n_j} \to \mathbb{R}^{n_{y_j}}$ describes the relation between state and measurement. We assume that the noise vectors $\mathbf{n}$ and $\mathbf{v}_j$ are independent mean-zero Gaussian random vectors.

In this paper, we consider situations where sensors can misdetect features and thus, do not produce a measurement at certain time instants. Examples include RF-based signals from beacons that are not detected by the agent because of low SNR, misdetection of features using cameras because of abrupt change of lighting conditions, no LIDAR returns from certain materials, etc. Under these circumstances, analogous to the Kalman Filter case (see equations (185) and (186) in [18]), an Extended Kalman Filter (EKF) based estimator of the state $\mathbf{x}$ can be written as:

$$\mathbf{P}_{t+1}^{-1} = (\mathbf{F}_t\mathbf{P}_t\mathbf{F}_t' + \mathbf{Q}_t)^{-1} + \sum_{j=1}^{m} \gamma_{j,t+1}\mathbf{H}_j'\mathbf{R}_{j,t+1}^{-1}\mathbf{H}_j, \tag{3}$$

$$\hat{\mathbf{x}}_{t+1} = \mathbf{P}_{t+1}\Big((\mathbf{F}_t\mathbf{P}_t\mathbf{F}_t' + \mathbf{Q}_t)^{-1}\mathbf{f}(\hat{\mathbf{x}}_t, \mathbf{0}) + \\ + \sum_{j=1}^{m} \gamma_{j,t+1}\mathbf{H}_j'\mathbf{R}_{j,t+1}^{-1}(\mathbf{y}_j(t+1) - \mathbf{h}_j(\mathbf{f}(\hat{\mathbf{x}}_t), \mathbf{0}))\Big),$$

where $\hat{\mathbf{x}}_t$ is the state estimate, $\mathbf{P}_t$ is the error covariance with respect to the process and sensor noise terms, $\mathbf{F}_t$ is the linearization of $\mathbf{f}$ around $(\hat{\mathbf{x}}_t, \mathbf{0})$ and $\mathbf{H}_j$ is the linearization of $\mathbf{h}_j$ around $(\mathbf{f}(\hat{\mathbf{x}}_t), \mathbf{0})$. The matrix $\mathbf{Q}_t$ is the process noise covariance and the $\mathbf{R}_{j,t+1}$ is the measurement noise covariance associated with the j-th sensor. The $\gamma_{j,t+1}$ are binary, $0/1$, random variables that model the misdetection process for the j-th sensor at time $t+1$.

Our goal is to build a novel BRM that trades off accuracy and robustness when sensors can stochastically be in misdetection mode during the mission. We will call this *Robust Belief Roadmap* or *RBRM*.

In this work, we make the following assumptions:

Assumption 2.1 (Misdetection map): For each sensor j, we can characterize the misdetection probability $(1 - p_j)$ at locations in the environment. □

Note that we are not requiring the knowledge of the p_j's for *all* sensors at *every* location in the environment. If this is not known for certain regions of the environment or for certain sensors, one either assume $p_j < 1$ (increasingly pessimistic as p_j decreases) or $p_j = 1$ (optimistic).

Assumption 2.2 (Independence): We assume the misdetections γ_j to be independent over time and between sensors. Specifically, the γ_j are Bernoulli random variables with p_j being the probability of $\gamma_j = 1$. □

For constant values of p_j's, Assumption 2.2 is common in the literature pertaining to the research area involving estimation with intermittent observations, e.g., see [19]. However, most results in this field are concerned with stability of the estimation algorithms, while our focus in this paper is to characterize the evolution of the estimation performance. Further, in our set-up, the parameters p_j of the random variables $\gamma_{j,t}$ in (3) are functions of the state $\mathbf{x}$, whereas in estimation literature, the state dependence is not explicitly considered for the sake of notational brevity.

Assumption 2.3 (Consistency): We assume that the state estimate $\hat{\mathbf{x}}_t$ follows the nominal trajectory for the vehicle. □

The last assumption implies that we have a reasonable nominal model for the motion of the vehicle, and that there exists a control action that keeps the state estimate $\hat{\mathbf{x}}_t$ close to the nominal trajectory (c.f. [3]). Our work is concerned with the level of confidence measured through $\mathbf{P}_t$ that we can obtain in our state estimate $\hat{\mathbf{x}}_t$.

With these assumptions, we address the following:

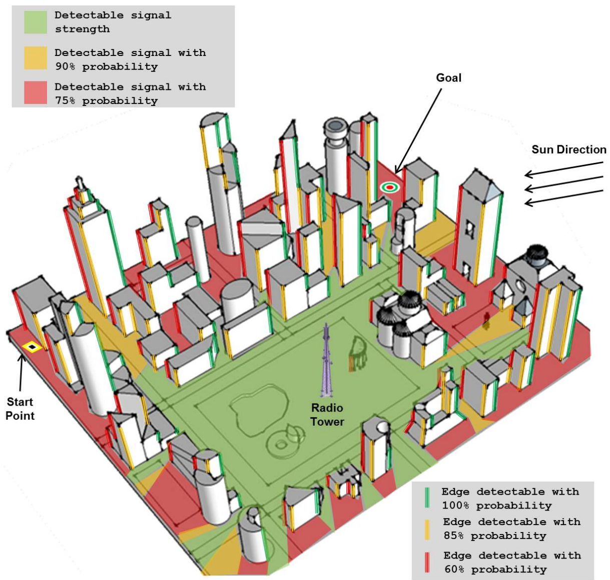

Fig. 1. Illustration of a model of the environment which could be used for planning. In this case, not only is the geometric information about the obstacles and position of beacons is considered, but also the information about the reliability of certain sensors in detecting, e.g. edges of buildings and signal from a radio tower (beacon). Note that in this scenario a rather elaborate model is used, where edges are categorized into three classes: detectable, detectable with 85% and 60% probability. This different detection likelihood could be caused by the sun's position. A map of signal strength from the radio tower could be determined using ray tracing algorithms. In this example, just for illustration purposes, we have three regions with different detection probabilities.

Problem 2.1: Given the sensors' precision, their misdetection probabilities and a nominal trajectory, determine a bound on the evolution of the expected value of $\mathcal{M}(\mathbf{P}_t)$, where $\mathcal{M}$ represents any function that can capture the uncertainty through $\mathbf{P}_t$. Here, the expectation is taken over the joint distribution of the random variables $\gamma_{j,t}$ representing sensor misdetection. □

Equipped with this theoretical bound, the second goal is to apply the bound to the following problem on path planning under uncertainty.

Problem 2.2: Given a set of candidate trajectories from a start location to a goal location, develop an algorithm that propagates the bound on $\mathbb{E}[\mathcal{M}(\mathbf{P}_t)]$ over the PRM, to output a path having minimum goal-state uncertainty. □

Remark 2.1: The probability of misdetection of a sensor (Assumption 2.1) is in general difficult to know precisely. However, thanks to rather realistic simulation environments capable of both simulating sensor responses as well as the environment, one can foresee the possibility of obtaining rather realistic models. For example, given a geometric model of the environment, edges and/or corners of buildings could be marked with different misdetection probabilities if some information from the type of material, the texture, the time of the day the mission is carried out, etc. are considered. Entire areas of the environment could be marked with misdetection probabilities, e.g., modeling the fact that an RF-signal cannot easily be detected behind buildings. This could be obtained with ray tracing based algorithms, see, e.g., Figure 1.

The misdetection probability of a sensor could also be determined from historical data collected in the mission, for example correlating some information about the environment, such as obstacle density, time of the day the mission was carried out, etc. with the misdetection state of a sensor.

Of course, it is impossible to capture all sources of uncertainty. However, if some of this information is available, the RBRM method can take it into consideration, trading off accuracy and robustness.

When such models are only of qualitative nature, the RBRM could be used to assess the robustness of the solution. In practice, the misdetection probabilities can be employed as user parameters. Varying such parameters, the user can study how the RBRM changes under, e.g., more pessimistic hypotheses on the behavior of certain sensors, having higher misdetection probability in more remote regions of the environment where more uncertainty is expected, etc. □

III. Analytical Bound on Performance

In the seminal work by Prentice and Roy [3], it was shown that if the covariance matrix is factorized as $\mathbf{P}_t = \mathbf{B}_t\mathbf{C}_t^{-1}$, then the time evolution of the terms $\mathbf{B}_t, \mathbf{C}_t$ is linear. This enabled the authors to develop and demonstrate a computationally efficient algorithm to compute a roadmap that captures the estimation precision. The function $\mathcal{M}$ used in [3] is the trace of the matrix. Leveraging the same factorization, one arrives at the following equation:

$$\begin{bmatrix}\mathbf{B}_t\\ \mathbf{C}_t\end{bmatrix} = \begin{bmatrix}\mathbf{F}_t & \mathbf{Q}_t\mathbf{F}_t^{-T}\\ \mathbf{M}(\gamma_t)\mathbf{F}_t & \mathbf{F}_t^{-T} + \mathbf{M}(\gamma_t)\mathbf{Q}_t\mathbf{F}_t^{-T}\end{bmatrix}\begin{bmatrix}\mathbf{B}_{t-1}\\ \mathbf{C}_{t-1}\end{bmatrix} \quad (4)$$

where $\mathbf{M}(\gamma_t) = \sum_{j=1}^{m}\gamma_{j,t}\mathbf{H}_j'\mathbf{R}_{j,t}^{-1}\mathbf{H}_j$, which depends on the stochastic variables $\gamma_{j,t}$. This can be thought as a transfer function that maps the matrices $\mathbf{B}_t$ and $\mathbf{C}_t$ from one node of the roadmap to the next [3]. In this stochastic setting, however, a direct application of the BRM proposed by Prentice and Roy in [3] requires extensive Monte Carlo simulations over all the variables $\gamma_{j,t}$. Even if the factorization provides a faster computation of the covariance, the method becomes very quickly intractable, especially if $\gamma_{j,t}$ changes spatially. See, e.g., the signal received from a radio tower as in Figure 1.

A way to mitigate this is by taking the expectation with respect to the $\gamma_{j,t}$, namely by computing $\mathbb{E}(\mathbf{B}_t)$ and $\mathbb{E}(\mathbf{C}_t)$. This would enable us to compute an expected transfer function between two nodes in the roadmap. However, note that $\mathbb{E}(\mathbf{P}_t) = \mathbb{E}(\mathbf{B}_t\mathbf{C}_t^{-1}) \neq \mathbb{E}(\mathbf{B}_t)(\mathbb{E}(\mathbf{C}_t))^{-1}$, thus preventing us from computing what the expected state covariance is at each node of the roadmap.

In order to obtain a meaningful metric on the expected error covariance, which captures the estimate precision when there are sensor misdetections, and to have computational tractability, we establish a bound on the largest eigenvalue of the covariance. Intuitively, we are approximating the uncertainty at each node of the roadmap with a ball whose radius is the largest eigenvalue of the covariance, and we determine a bound on this radius.

A. Bound under Stochastic Sensor Misdetections

In this section, we derive a bound on the expected maximum eigenvalue of the covariance under a misdetection process as per Assumptions 2.1 and 2.2. The metric which we analyze is $\mathbb{E}[\bar{\lambda}(\mathbf{P}_t)]$, where the expectation is taken over the stochastic process of sensor misdetections.

For brevity, let $\ell_t := \bar{\lambda}(\mathbf{P}_t)$. For $k \in \{1, \dots, m\}$, define:

$$a := \bar{\lambda}^2(\mathbf{F}(\hat{\mathbf{x}}_t)), \qquad b := \sup_t \bar{\lambda}(\mathbf{Q}_t),$$

$$c_{i_1,\dots,i_k} := a\underline{\lambda}\Big(\sum_{j=1}^{k} \mathbf{H}'_{i_j,t}\mathbf{R}^{-1}_{i_j,t}\mathbf{H}_{i_j,t}\Big),$$

$$d_{i_1,\dots,i_k} := bc_{i_1,\dots,i_k}/a + 1,$$

where a tuple $i_1, \dots, i_k$ is a subset of $\{1, \dots, m\}$.

Using this notation, we have the following recursion which provides an upper bound on $\mathbb{E}[\ell_t]$, referred to hereafter as $\overline{\mathbb{E}[\ell_t]}$. Due to lack of space, the proof of this result is included in the appendix of [20][Proof of Theorem III.3].

Theorem 3.1 (Stochastic misdetections): Under Assumptions 2.1 and 2.2, at any given time instant t, $\overline{\mathbb{E}[\ell_t]}$ generated as per the following recursion,

$$\begin{aligned}\overline{\mathbb{E}[\ell_t]} &= (a\overline{\mathbb{E}[\ell_{t-1}]} + b)\Big((1-p_1)\dots(1-p_m)\\ &+ \frac{p_1(1-p_2)\dots(1-p_m)}{c_1\overline{\mathbb{E}[\ell_{t-1}]} + d_1} + \dots + \frac{(1-p_1)(1-p_2)\dots p_m}{c_m\overline{\mathbb{E}[\ell_{t-1}]} + d_m}\\ &+ \frac{p_1p_2\dots(1-p_m)}{c_{12}\overline{\mathbb{E}[\ell_{t-1}]} + d_{12}} + \dots + \frac{(1-p_1)\dots p_{m-1}p_m}{c_{m-1,m}\overline{\mathbb{E}[\ell_{t-1}]} + d_{m-1,m}}\\ &\vdots\\ &+ \frac{p_1\dots p_m}{c_{1,\dots,m}\overline{\mathbb{E}[\ell_{t-1}]} + d_{1,\dots,m}}\Big),\end{aligned}$$

is an upper bound on $\mathbb{E}[\ell_t]$. □

This bound requires the enumeration of all of the 2^m possibilities of sensor combinations, and therefore, the computational complexity scales undesirably with m. One way to derive an efficient bound is to obtain a uniform lower bound $\bar{c}$ on each of the c's. In that case, the common denominator of the right hand side terms becomes $\bar{c}\,\mathbb{E}[\ell_{t-1}] + \bar{d}$. The recursion then simplifies to

$$\overline{\mathbb{E}[\ell_t]} = (a\overline{\mathbb{E}[\ell_{t-1}]} + b)\left(\prod_{j=1}^{m} q_j + \frac{1 - \prod_{j=1}^{m} q_j}{\bar{c}\,\overline{\mathbb{E}[\ell_{t-1}]} + \bar{d}}\right),$$

with $q_j = 1 - p_j$. This recursion can be evaluated along similar lines to the proof of [20][Theorem III.2] to obtain a $\overline{\mathbb{E}[\ell_t]}$ as a function of $\mathbb{E}[\ell_0]$.

For certain types of sensor suites, one may be able to derive a slightly conservative, but computationally efficient upper bound which we report next.

Corollary 3.1 (Simplified bound): Under Assumptions 2.1 and 2.2, at any given time instant t, $\overline{\mathbb{E}[\ell_t]}$ generated as per the following recursion,

$$\overline{\mathbb{E}[\ell_t]} = (a\overline{\mathbb{E}[\ell_{t-1}]}+b)\left(\prod_{j=1}^{m} q_j + \sum_{j=1}^{m}\frac{p_j}{c_j\overline{\mathbb{E}[\ell_{t-1}]} + d_j}\right),$$

is an upper bound on $\mathbb{E}[\ell_t]$. □

The proof is reported in [20]. The main advantage of this bound is the computational efficiency as compared to the one in Theorem 3.1. However, this bound requires at least one of the sensors to have a strictly positive c value, and therefore, may become too conservative. We will use Theorem 3.1 in our proposed RBRM approach.

IV. Application to Path Planning Missions

The upper bound on $\mathbb{E}[\ell_t]$ given in Theorem 3.1 may be used to plan paths of minimum expected goal-state uncertainty in a manner similar to the belief roadmap algorithm [3]. We will assume that a probabilistic roadmap with node set N and edge set E is provided as input, along with beliefs μ_0 and μ_{goal} defining a start state and goal state on the roadmap. We also assume that for every node $n \in N$, the triple $n = \{\mu, \overline{\mathbb{E}[\ell]}, \pi\}$ is stored, which contains the belief, the eigenvalue bound, and the path π (beginning at μ_0) associated with this node. We refer to individual members of the triple using the notation $n[\mu]$, $n[\overline{\mathbb{E}[\ell]}]$, and $n[\pi]$. Belief propagation and graph search proceeds similarly to that of the standard BRM algorithm; $\overline{\mathbb{E}[\ell_t]}$ is propagated according to the recursive inequality given in Theorem 3.1, and is used in place of the nominal-trajectory expected error covariance matrix that is propagated in the standard BRM. We assume the bound is used to compute a transfer function $\overline{\mathbb{E}[\ell]}_l = \zeta(i, l, \overline{\mathbb{E}[\ell]}_i)$, that takes as input the indices of an edge $e_{i,l}$ in the roadmap, and the eigenvalue bound associated with node n_i. In the context of the graph search, we treat $\overline{\mathbb{E}[\ell]}$ independently of time, and assume that $n_i[\overline{\mathbb{E}[\ell]}]$ represents the best-yet covariance eigenvalue bound identified at n_i. The search process is shown in Algorithm 1.

Algorithm 1 $n_{goal}[\pi] = RBRM(\mu_0, \mu_{goal}, \overline{\mathbb{E}[\ell]}_0, N, E)$

```
for e_{i,l} ∈ E do
  ξ(i, l, E[ℓ]_i) ← PropagateBound(e_{i,l})
end for
Q ← n_0 = {μ_0, E[ℓ]_0, ∅}
while Q ≠ ∅ do
  n_i ← Pop(Q)
  for n_l ∈ e_{i,l} do
    if n_l ∉ n_i[π] then
      E[ℓ]_l ← ξ(i, l, n_i[E[ℓ]])
      if E[ℓ]_l < n_l[E[ℓ]] then
        n_l ← {n_l[μ], E[ℓ]_l, n_i[π] ∪ n_l}
        Q ← Push(Q, n_l)
      end if
    end if
  end for
end while
return n_goal[π]
```

The use of our proposed approach, i.e., propagation of $\overline{\mathbb{E}[\ell_t]}$, provides us with a significant computational advantage over existing methods such as [3]. If we were to use their factorization from (4), then we would have to compute:

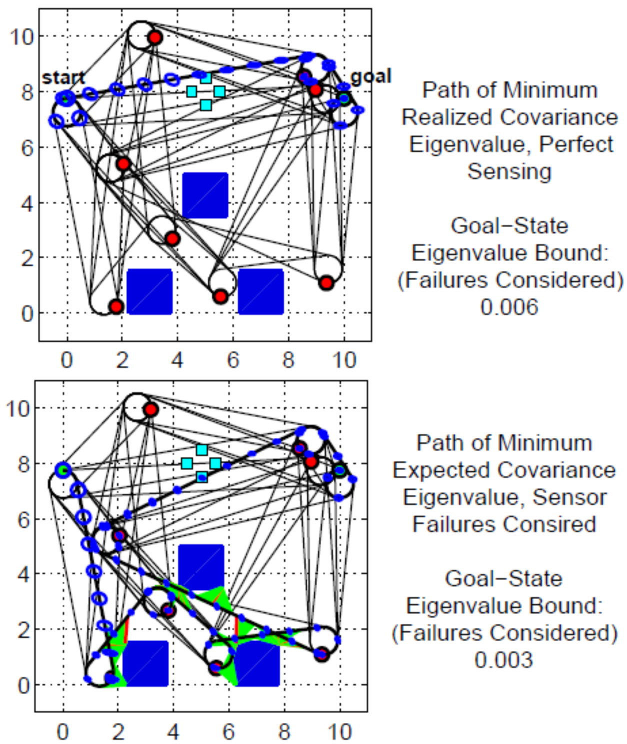

Fig. 2. Planned paths in a workspace populated with obstacles (measured by laser) and UWB beacons. The robot receives the beacon measurements with probability 0.1, and extracts obstacle corners from laser data with probability 0.9. At top, a path planned using ℓ_t as a performance metric, neglecting all probabilistic sensor misdetections. At bottom, a path planned using $\overline{\mathbb{E}[\ell_t]}$ as a performance metric, which considers the misdetection probability of each sensor. The UWB beacons are queried at every measurement iteration; the laser has a range of one unit and its planned measurements are rendered (green for a successful measurement and red for a misdetection) for a representative failure scenario. Ninety-five percent confidence covariance ellipses are plotted at regular intervals along each path.

1) 2^m realizations of the matrix $\mathbf{B}_t$ (one for each subset of misdetecting sensors), 2) inverses of 2^m realizations of the matrix $\mathbf{C}_t$, 3) multiply each realization of $\mathbf{B}_t$ with corresponding $\mathbf{C}_t^{-1}$ and finally, 4) sum up the 2^m terms to compute $\mathbb{E}[\mathbf{P}_t]$ or its trace. Instead, our approach requires the computation of minimum eigenvalues of 2^m much smaller sized matrices, i.e., sums of the terms $\mathbf{H}_j'\mathbf{R}_{j,t}^{-1}\mathbf{H}_j$, for which efficient algorithms exist even for larger sizes [21], along with step 4) of the above, which provides significant savings in high dimensional state space.

V. Computational Results

In this section, we consider path planning with minimum uncertainty under process noise, sensor noise, and probabilistic misdetections for a planar Dubins vehicle [22] in an environment populated with obstacles. We assume that a robot is using three sensors for navigation: ultra-wideband (UWB) range beacons, a laser rangefinder for measuring obstacle vertices, and odometry that is subject to drift over time. The beacons provide measurements throughout the workspace, but their noise properties are assumed to vary

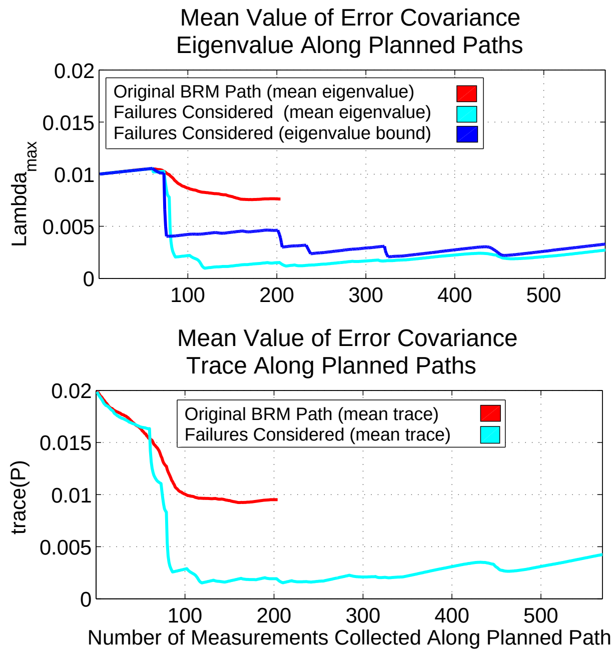

Fig. 3. At top, the propagation in time of the eigenvalue performance metrics over the paths in Figure 2. At bottom, $tr(\mathbf{P}_t)$ is also given for both paths. All quantities except $\overline{\mathbb{E}[\ell_t]}$ represent the mean over one hundred Monte Carlo trials in which different sequences of sensor misdetections occur according to the prescribed probabilities.

as a function of distance to the robot[1], according to

$$\mathbf{v}_j(t) \sim \mathcal{N}(0, \sigma(D_j(t))^2)\,, \tag{5}$$

$$\sigma(D_j(t)) = \alpha D_j(t) + \sigma_0\,. \tag{6}$$

The noise associated with the range measurement of beacon j has a standard deviation that varies linearly in the Euclidean distance $D_j(t)$ between the robot and beacon j. The standard deviation takes on value σ_0 at range zero and increases according to the coefficient α. For the laser rangefinder, we assume the measurement of range to an obstacle vertex is corrupted by Gaussian white noise with properties that do not vary spatially, and the vertices measured are always correctly associated with a prior map. The maximum range of the laser is limited, however, and obstacles can only be detected in close proximity to the robot.

A start state and goal state are designated for the robot, and a PRM is used to identify feasible paths between the start and goal. To select the path of minimum goal-state uncertainty, two methodologies are compared: the original BRM algorithm, with no notion of sensor misdetections, and the proposed RBRM algorithm, which uses $\overline{\mathbb{E}[\ell_t]}$ as a cost metric instead of $tr(\mathbf{P}_t)$. For all path planning scenarios investigated, the standard BRM algorithm was found to choose the same path regardless of whether $tr(\mathbf{P}_t)$ is used as the cost metric or ℓ_t is used instead. Evaluating ℓ_t over the roadmap offers a better comparison with $\overline{\mathbb{E}[\ell_t]}$, and so

[1]A more general model could also consider a bias term as described in [3]. This could be easily added also in our framework.

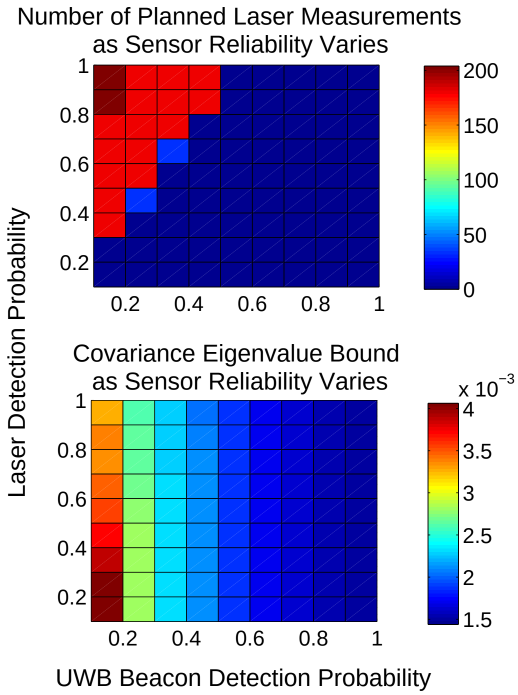

Fig. 4. Characteristics of a planned path are plotted as a function of sensor reliability, for the two-sensor example shown in Figure 2. At top, the covariance eigenvalue bound at the goal state is illustrated, and at bottom, the number of planned laser measurements along the selected path is illustrated. The upper left corner of each plot corresponds to the parametrization used in Figures 2 and 3.

both $tr(\mathbf{P}_t)$ and ℓ_t are computed for comparison with $\overline{\mathbb{E}[\ell_t]}$ in the results to follow.

The first scenario considered is illustrated in Figure 2, in which a robot must plan from start to goal in a workspace populated with three obstacles and four range beacons. Very simple collision-free paths are evident through the upper reaches of the workspace, but in cases where the probability of UWB misdetection is high, it is advantageous for the robot to travel through the obstacles to collect laser measurements that reduce position uncertainty. For the specific case plotted in Figure 2, the beacons have a ten percent probability of delivering a successful measurement to the robot, and the laser (with a maximum range of one unit) has a ninety percent probability of successfully extracting an obstacle vertex and measuring its range to the robot. When intermittent sensing is neglected, the robot takes a short path to the goal that collects measurements from the UWB beacons only. When intermittent sensing is considered, the robot takes a detour through the obstacles to reduce the uncertainty of its state estimate. For both paths, one hundred Monte Carlo simulations were performed in which sensors fail according to the prescribed probabilities, and the resulting mean values of $tr(\mathbf{P}_t)$ and ℓ_t are compared with $\overline{\mathbb{E}[\ell_t]}$ in Figure 3.

The same planning scenario is next considered over a range of different misdetection probabilities, for both the laser and the UWB beacons, and the results are summarized in Figure 4. The number of planned laser measurements in the minimum uncertainty path, computed using $\overline{\mathbb{E}[\ell_t]}$, is given at top, and the value of $\overline{\mathbb{E}[\ell_t]}$ at each path's goal state is given at bottom. The zero-range noise level σ_0^2 selected for the UWB beacons is an order of magnitude lower than the constant variance representing the laser noise, and so the UWB beacons are used exclusively for all scenarios in which they are more than fifty percent reliable, even if the laser is more reliable. Note that Figure 4 can be also used when no exact value of the misdetection probabilities is known, to evaluate the characteristics of a PRM over an environment. Note that to explore tradeoffs the proposed approach is very efficient as the parameters $a, b, c_{i_1}, \ldots, c_{i_k}$ and $d_{i_1}, \ldots, d_{i_k}$ need to be computed only once, and after that we only need to propagate a scalar metric across a PRM.

A second path planning test case with continuously varying sensor intermittency is considered in Figure 5. In a workspace populated with eight obstacles and no UWB beacons, we assume that a light source causes the expected sensing intermittency to vary continuously along the vertical axis of the workspace, with a high detection probability at bottom and a low detection probability at top. Neglecting sensor intermittency, the standard BRM algorithm plans a path through the upper region of the workspace, and considering sensor intermittency, planning with $\overline{\mathbb{E}[\ell_t]}$ yields a path that collects many high-probability measurements from the lower region of the workspace to minimize uncertainty at the goal state. The candidate metrics, averaged over one hundred simulated cases of sensor intermittency, are given in Figure 6.

A final path planning test case is considered in Figure 7, which plans over a square-kilometer urban environment (from the city of Chicago) from a start state at bottom to a goal state at top. We assume that sunlight is cast into the environment from the upper right corner of the map, interfering with the robot's ability to detect features with a laser in the sunlit areas. We assume that blue obstacle corners in Figure 7, which lie in shaded areas, can be detected by laser with 90% probability, and red obstacle corners, in sunlit areas, can be detected with 10% probability. We believe that this reflects a realistic application in which prior knowledge can be applied to plan with increased robustness. We use only two feature detection probabilities in this case to reflect the fact that we may not know exactly how the reliability of sensing will vary along a continuum.

Neglecting sensor intermittency, the standard BRM algorithm plans a path that relies on many obstacle corners with a low detection probability. Using $\overline{\mathbb{E}[\ell_t]}$ as a planning metric instead, we obtain a path that collects measurement from the highly reliable features exclusively. This path reaches the goal state with superior uncertainty in the majority of test cases, and is more robust in general due to its preference for reliable features. The candidate metrics, again averaged over one hundred simulated cases of sensor intermittency for this example, are given in Figure 8.

Over the course of computational evaluations, we have also observed that using $\overline{\mathbb{E}[\ell_t]}$ as an uncertainty metric for planning, even in the absence of sensor misdetection, offers

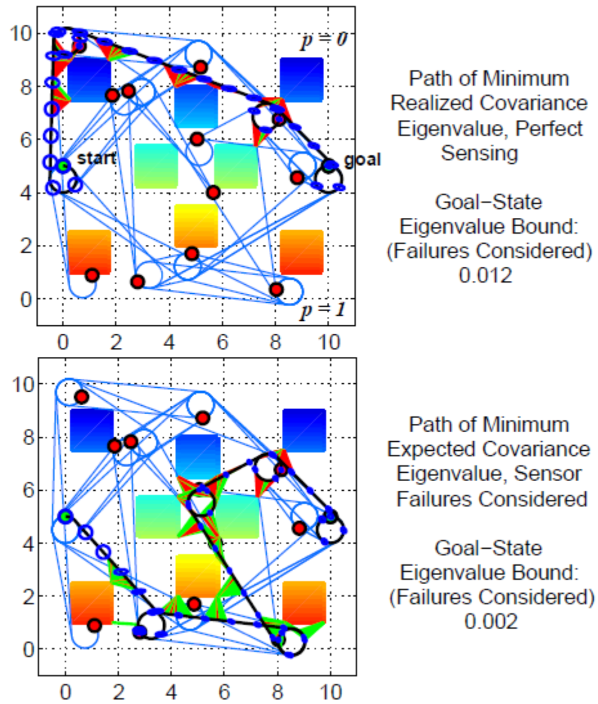

Fig. 5. Planned paths in a workspace over which the probability of a successful corner detection varies spatially along the vertical axis. Obstacles measured at bottom have the highest probability of a successful measurement, and obstacles measured at top have a near-zero probability of a successful measurement. At top, a path planned using ℓ_t as a performance metric, neglecting all probabilistic sensor misdetections. At bottom, a path planned using $\mathbb{E}[\ell_t]$ as a performance metric, which considers the misdetection probability of each sensor. The laser has a range of one unit and its planned measurements are rendered (green for a successful measurement and red for a misdetection) for a representative scenario. Ninety-five percent confidence covariance ellipses are plotted at regular intervals along each path.

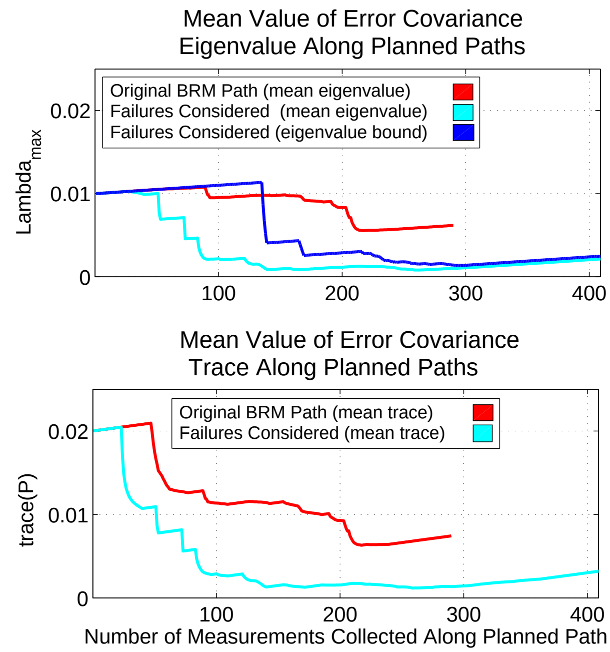

Fig. 6. At top, the propagation in time of the eigenvalue performance metrics over the paths in Figure 5. At bottom, the trace of the expected error covariance matrix is given for both paths. All quantities except the eigenvalue bound represent the mean over one hundred Monte Carlo trials in which different sequences of sensor misdetections occur according to the prescribed probabilities.

a competitive and computationally efficient alternative to propagation of the full error covariance matrix. As Figure 8 indicates, the eigenvalue bound is not always tight when the vehicle relies solely on odometry, and its state estimate is subject to drift, but $\mathbb{E}[\ell_t]$ offers a good approximation of ℓ_t, which we believe is in turn a suitable proxy for $tr(\mathbf{P}_t)$.

VI. Conclusion and Future Directions

This paper described how to plan when sensors used for state estimation are not only noisy, but may also fail to produce measurements because of misdetections. Being able to tradeoff both accuracy and robustness is very appealing as autonomous vehicles heavily rely on complex sensors such as cameras and LIDAR whose capability of extracting relevant information, such as features and point clouds, strongly depends on environmental information that can be predicted to a certain extent, such as effect of lighting conditions, type of surfaces, etc. Even in the case when such information is not fully available, the proposed methodology can be very beneficial to study the robustness of the path to intermittent sensing, by testing the robust roadmap, for example, by choosing various probabilities of intermittency at various locations in the map.

One direction in which the framework proposed in this paper needs to be matured is when uncertainty can be tolerated in certain dimensions but not in others. These scenarios arise in planning trajectories in high dimensional robot configuration spaces. The goal is to develop extensions of the current formulation and an analysis framework that can inherently handle such preferred directions for uncertainty. Other promising short term future directions include the incorporation of map uncertainty within the current framework and the use of the current analysis for multi-objective path planning.

References

[1] R. Alterovitz, T. Simeon, and K. Goldberg, "The stochastic motion roadmap: A sampling framework for planning with Markov motion uncertainty," in *Proceedings of the Robotics: Science and Systems Conference*, 2007.

[2] B. Marthi, "Robust navigation execution by planning in belief space," in *Proceedings of the Robotics: Science and Systems Conference*, 2008.

[3] S. Prentice and N. Roy, "The belief roadmap: Efficient planning in belief space by factoring the covariance," *International Journal of Robotics Research*, vol. 28, no. 11–12, pp. 1448–1465, 2009.

[4] L. E. Kavraki, P. Svestka, J.-C. Latombe, and M. H. Overmars, "Probabilistic roadmaps for path planning in high-dimensional configuration spaces," *IEEE Transactions on Robotics*, vol. 12, no. 4, pp. 556–580, 1996.

[5] A. Gelb, Ed., *Applied Optimal Estimation*. MIT Press, 1974.

[6] R. He, S. Prentice, and N. Roy, "Planning in information space for a quadrotor helicopter in a GPS-denied environment," in *Proceedings of the IEEE International Conference on Robotics and Automation*, 2008, pp. 814–820.

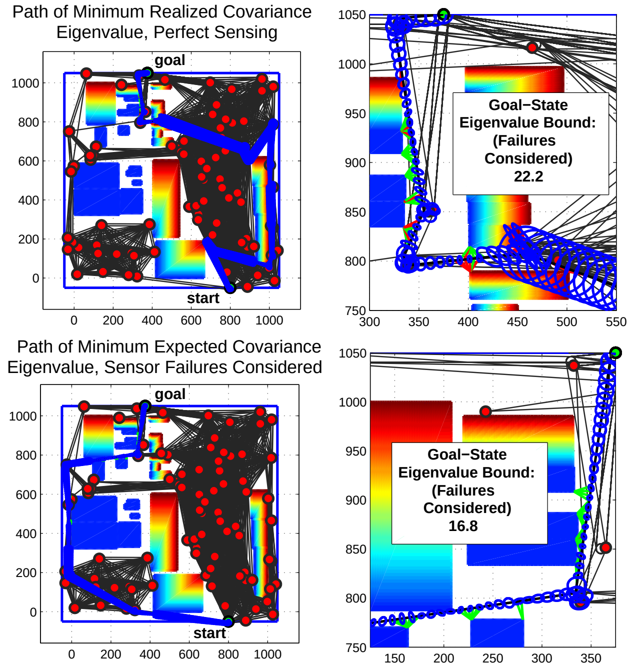

Fig. 7. Planned paths in a square-kilometer workspace in which the probability of a successful corner detection by laser varies due to sunlight originating in the upper right corner of the map. Sunlit portions of the obstacles, indicated in red, have a 10% probability of a successful measurement. Shaded portions of the obstacles, indicated in blue, have a 90% probability of a successful measurement. At top left, a path planned using ℓ_t as a performance metric, neglecting all probabilistic sensor misdetections. At bottom left, a path planned using $\mathbb{E}[\ell_t]$ as a performance metric, which considers the misdetection probabilities. The laser has a range of twenty meters and its planned measurements are rendered (green for a successful measurement and red for a misdetection) for a representative scenario. Ninety-five percent confidence covariance ellipses are plotted in blue at regular intervals along each path. The top left and bottom left paths are shown in increased detail at top right and bottom right, respectively.

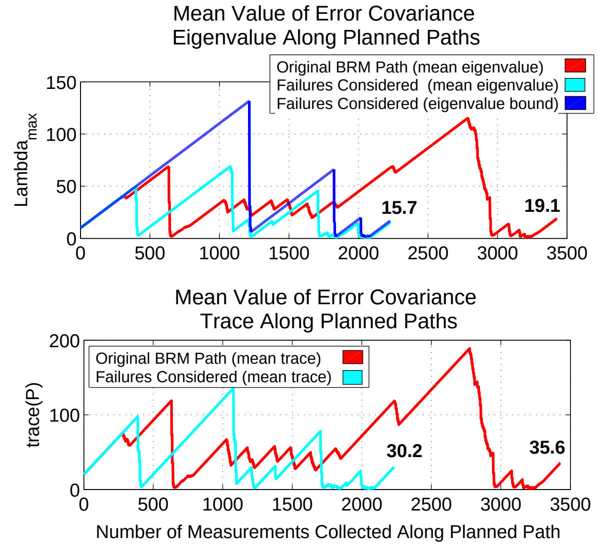

Fig. 8. At top, the propagation in time of the eigenvalue performance metrics over the specific paths in Figure 7. At bottom, the trace of the expected error covariance matrix is given for both paths. All quantities except the eigenvalue bound represent the mean over one hundred Monte Carlo trials in which different sequences of sensor misdetections occur according to the prescribed probabilities.

[7] H. Takeda, C. Facchinetti, and J.-C. Latombe, "Planning the motions of a mobile robot in a sensory uncertainty field," *IEEE Transactions on Pattern Analysis and Machine Intelligence*, vol. 16, no. 10, pp. 1002–1017, 1994.

[8] A. Bry and N. Roy, "Rapidly-exploring random belief trees for motion planning under uncertainty," in *Proceedings of the IEEE International Conference on Robotics and Automation*, 2011.

[9] S. Karaman and E. Frazzoli, "Sampling-based algorithms for optimal motion planning," *International Journal of Robotics Research*, vol. 30, no. 7, pp. 846–894, 2011.

[10] J. van den Berg, P. Abbeel, and K. Goldberg, "LQG-MP: Optimized path planning for robots with motion uncertainty and imperfect state information," *International Journal of Robotics Research*, vol. 30, no. 7, pp. 895–913, 2011.

[11] S. M. LaValle and J. J. Kuffner, "Randomized kinodynamic planning," *International Journal of Robotics Research*, vol. 20, no. 5, pp. 378–400, 2001.

[12] R. P. Jr., R. Tedrake, L. Kaelbling, and T. Lozano-Perez, "Belief space planning assuming maximum likelihood observations," in *Proceedings of Robotics: Science and Systems Conference*, 2010.

[13] H. Kurniawati, T. Bandyopadhyay, and N. M. Patrikalakis, "Global motion planning under uncertain motion, sensing, and environment map," in *Proceeding of Robotics: Science and Systems Conference*, 2011.

[14] M. P. Vitus, W. Zhang, and C. Tomlin, "A hierarchical method for stochastic motion planning in uncertain environments," in *Proceedings of the IEEE/RSJ International Conference on Intelligent Robots and Systems*, 2012.

[15] M. P. Wellman, M. Ford, and K. Larson, "Path planning under time-dependent uncertainty," in *Proceedings of the Eleventh Conference on Uncertainty in Artificial Intelligence*, 1995.

[16] E. U. Acar, H. Choset, Y. Zhang, and M. Schervish, "Path planning for robotic demining: Robust sensor-based coverage of unstructured environments and probabilistic methods," *International Journal of Robotics Research*, vol. 22, no. 7-8, pp. 441–466, 2003.

[17] W. H. Kwon, Y. Moon, and S. C. Ahn, "Bounds in algebraic Riccati and Lyapunov equations: A survey and some new results," *Int. Jour. of Control*, vol. 64, no. 3, 1996.

[18] H. Durrant-Whyte, "Multi sensor data fusion," http://www.acfr.usyd.edu.au/pdfs/training/multiSensorDataFusion/dataFusionNotes.pdf, 2001.

[19] B. Sinopoli, L. Schenato, M. Franceschetti, K. Poolla, M. Jordan, and S. S. Sastry, "Kalman filtering with intermittent observations," *IEEE Transactions on Automatic Control*, vol. 49, no. 9, pp. 1453–1464, 2004.

[20] S. D. Bopardikar, B. J. Englot, and A. Speranzon, "Robust belief roadmap: Planning under intermittent sensing," 2013, http://arxiv.org/abs/1304.7256.

[21] Y. Okamoto and H. J. Maris, "A novel algorithm for calculation of the extreme eigenvalues of large Hermitian matrices," *Computer Phy. Comm.*, vol. 76, no. 2, 1993.

[22] L. E. Dubins, "On curves of minimal length with a constraint on average curvature, and with prescribed initial and terminal positions and tangents," *American Journal of Mathematics*, vol. 79, no. 3, pp. 497–516, 1957.